The jet centerline pressures for all three supersonic flow cases are given in Fig. 3. The centerline pressure distributions show that, in all three cases, the pressure oscillations diminish rapidly after the first shock cell.

C. Mach 6 Jet in a Mach 5 Freestream

The primary goal of the present work is to understand the structures of hypersonic jets. Toward this end, a Mach 6 jet in a Mach 5 freestream is studied. Three jet-to-ambience pressure ratios are considered; they are p_j/p_a = 3, 5, and 10.

The present results show that the basic structure of a hypersonic jet is similar to that of a supersonic jet. All of the previous analyses about supersonic jets also apply here. The major distinct features for jets in the hypersonic regime are that the cell lengths are much longer, the shocks and expansion waves induced in the freestream by the jet stay fairly close to the boundary of the jet, and, therefore, the exit shock tends to merge with the shear layer of the jet boundary, thus making it a layer of rapid changing pressure and rapid changing velocity.

The centerline pressure distributions for the three hypersonic jet cases mentioned earlier are given in Fig. 4. A comparison between Figs. 3 and 4 shows that as the flight Mach number increases, the oscillation in the centerline pressure behind the first cell decreases.

IV. Concluding Remarks

The present numerical study demonstrates that the phenomenon of underexpanded jets can be analyzed using full Navier-Stokes solvers without resorting to special treatments of the jet flowfield. It also shows that the jet structures are considerably different for subsonic and supersonic ambient flows. A supersonic pressure relief effect has been identified. This pressure relief effect reduces the pressure oscillation in an underexpanded jet in supersonic ambient flows. The study also shows that the length scales in hypersonic jets are considerably different from those in supersonic jets.

References

[1]Seiner, J. M., and Norun, T. D., "Experiments of Shock Associated Noise on Supersonic Jets," AIAA Paper 79-1526, July 1979.

[2]Chiang, C.-H., "Axially Symmetric Supersonic Turbulent Jets Discharged from a Nozzle with Underexpansion," *Turbulent Jets of Air, Plasma, and Real Gas,* Consultants Bureau, New York, 1969.

[3]Chuech, S. G., Lai, M.-C., and Faeth, G. M., "Structure of Turbulent Sonic Underexpanded Jets," AIAA Paper 88-0700, Jan. 1988.

[4]Reid, J., and Hasting, R. C., "The Effect of a Central Jet on the Base Pressure of a Cylindrical After-body in a Supersonic Stream," Aeronautical Research Council, London, Rept. and Mem. 3224, 1961.

[5]Salas, M. D., "The Numerical Calculation of Inviscid Plume Flowfields," AIAA Paper 74-523, June 1974.

[6]Dash, S. M., Pearce, B. E., Pergament, H. S., and Fichburne, E. S., "Prediction of Rocket Plume Flowfields for IR Signatures Studies," *Journal of Spacecraft and Rockets,* Vol. 17, May-June 1980, pp. 190–199.

[7]Dash, S. M., and Thorpe, R. D., "A Shock Capturing Model (SCIPPY) for the Analysis of Steady Supersonic One and Two Phase Flows," AIAA Paper 80-1254, June 1980.

[8]Dash, S. M., and Wolf, D. E., "Interactive Phenomena in Supersonic Jet Mixing Problems," *AIAA Journal,* Vol. 22, July 1984, pp. 905–913.

[9]Dash, S. M., Wolf, D. E., and Seiner, J. M., "Analysis of Turbulent Underexpanded Jets, Part I: Parabolized Navier-Stokes Model, SCIPVIS," *AIAA Journal,* Vol. 24, April 1985, pp. 505–514.

[10]Pulliam, T. H., and Steger, J. L., "Implicit Finite-Difference Simulations of Three-Dimensional Compressible Flow," *AIAA Journal,* Vol. 18, Feb. 1980, pp. 159–167.

[11]Cooper, G. K., "The PARC Codes," Arnold Engineering Development Center Rept., Tullahoma, TN, Sept. 1986.

[12]Hsu, A. T., and Lytle, J. K., "A Simple Algebraic Grid Adaptation Scheme with Applications to Two- and Three-Dimensional Flow Problems," *Proceedings of the AIAA 9th Computational Fluid Dynamics Conference,* AIAA, Washington, DC, June 1989.

Propellant Feed System of a Regeneratively Cooled Scramjet

Takeshi Kanda,* Goro Masuya,† and Yoshio Wakamatsu†
National Aerospace Laboratory, Miyagi, Japan

Nomenclature

F = thrust, N
h = height of the inlet
Isp = specific impulse, $m \cdot s^{-1}$
M = Mach number
$\dot{m}$ = mass flow rate, $kg \cdot s^{-1}$

Subscripts

cl = coolant
H2 = hydrogen
st = stoichiometric
∞ = freestream

I. Introduction

THERE is great interest in the use of scramjets as engines for aerospace planes, but there have been few reports[1-3] on scramjet engine cycles, in other words, propellant supply systems. Therefore, the feasibility of scramjet engine cycles has not been made clear, and potential problems in scramjet development remain unclear. To address this deficiency, a cycle analysis has been conducted of an airframe-integrated hydrogen-fueled scramjet engine.

The flight path of the vehicle is along a constant dynamic pressure of 100 kPa. The range of flight Mach numbers is from 6–12.

II. Assumptions and Methods of Calculation

A. Engine Cycle Schematic and Configuration

An expander cycle is adopted as a fuel supply system (see Fig. 1). The turbine is driven by gaseous hydrogen that is heated while regeneratively cooling the engine. The six scramjet engine modules are mounted on a vehicle. Each component of the air breathing part, e.g., the combustor, is cooled individually. The frontal area of the inlet of each module is 1 m^2. The length from the entrance of the inlet to the exit of the inner nozzle is 7.7 m.

In principle, the equivalence ratio in the combustor is kept at unity. When the hydrogen flow rate required for engine cooling exceeds the stoichiometric flow rate, all of the hydrogen required for cooling is injected into the combustor. The engine overall thrust and the specific impulse with stoichiometric combustion are referred to as the reference values in the discussion.

B. Properties of Combustion Gas

The temperature, pressure, speed, and specific impulse in the air breathing part are calculated using a quasi-one-dimensional model with friction, combustion, and heat transfer.[4] In the model, the following methods and assumptions are used:

1) The vehicle forebody is approximated by a cone. The results with the cone's half-angle of 5 deg are referred to here.

Received Aug. 8, 1989; accepted for publication Sept. 14, 1989.

*Researcher, Kakuda Branch.
†Senior Researcher, Kakuda Branch.

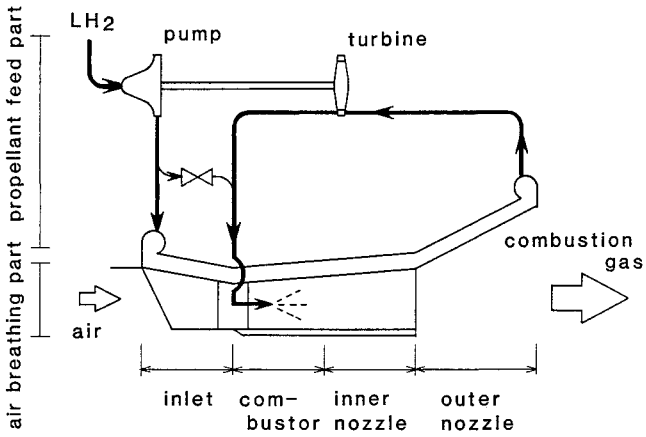

Fig. 1 Engine cycle schematic—expander cycle.

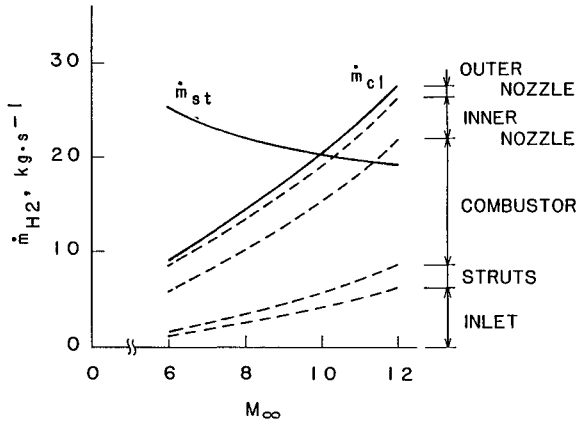

Fig. 2 Fuel flow rate.

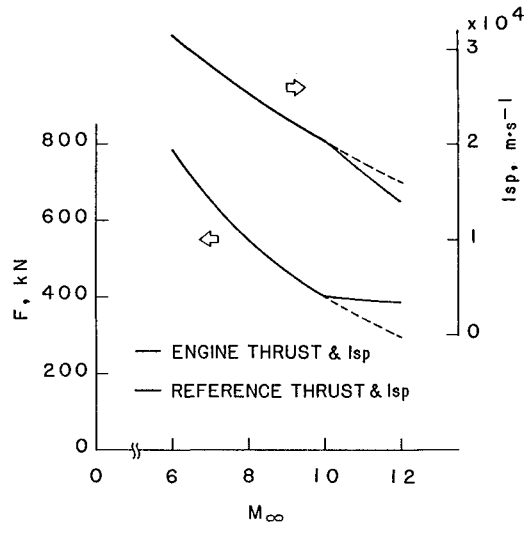

Fig. 3 Engine overall thrust and specific impulse.

2) The friction coefficient is assumed constant, and the Reynolds analogy is adopted to calculate heat transfer.

3) In the inlet, experimental correlations[5] of pressure recovery ratio and of capture area ratio are used.

4) In the outer nozzle, the exhaust gas is assumed to expand to the same pressure as that around the forebody. Nozzle efficiency based on impulse increment is assumed to be 0.98.

C. Cycle Balance

When the power required by the pump becomes equal to the power produced by the turbine,[6] the cycle is balanced. With reference to rocket engines, we assume the efficiency of the turbopump to be 0.36.[7] The fuel/air dynamic pressure ratio at the injector orifices is set at unity based on the results of a previous experiment.[8]

D. Heat Transfer and Coolant Pressure Loss

Because overall heat absorbed by the coolant is important in the cycle power balance calculation, the effect of peak heat flux at the leading edge is neglected. The heat flux on the hot gas side is calculated with the heat transfer coefficient of Mayer.[9] The wall temperature on the hot gas side is fixed uniformly for simplicity.

The wall is assumed to be nickel alloy. The wall temperature on the hot gas side is set at 1000 K, and the hydrogen temperature at the cooling jacket exit is set at 700 K because of the high temperature strength of nickel alloy.

The pressure loss inside the regenerative cooling channels as the result of both friction[6] and expansion of heated coolant[6] is considered. The other pressure losses at the manifolds and the injector channel are also considered. These pressure losses are nondimensionalized by the injector manifold pressure, and their values are taken from the values of rocket engines.[7]

III. Results and Discussion

A. Hydrogen Flow Rate

The flow rates in Fig. 2 are the total amount of six modules. The breakdown of the cooling in each component is shown at the right side in the figure.

Sufficient heat transfer to establish the expander cylinder is gained from the regenerative cooling of the scramjet because of its broad wetted area. The pump exit pressure is about 3 MPa at Mach 6 and about 7 MPa at Mach 12.

The flow rate for cooling $\dot{m}_{cl}$ increases as the flight Mach number M_∞ increases. A similar result was obtained by Buchmann.[1] The pump feeds the stoichiometric flow rate $\dot{m}_{st}$ when the cooling flow rate is less than the stoichiometric flow rate but has to feed the extra hydrogen for cooling at flight Mach numbers greater than 10.

B. Engine Overall Thrust and Specific Impulse

The engine overall thrust and the specific impulse are shown in Fig. 3. Below Mach 10, the thrust and the specific impulse coincide with the reference values. At flight Mach numbers above 10, a reduction of the specific impulse occurs because of the coolant flow rate requirement, which is accompanied by an increase of the thrust. It is possible to increase the thrust by injecting excess fuel into the combustor to compensate for the decrease of the specific impulse.

IV. Summary

An expander cycle for an airframe-integrated hydrogen-fueled scramjet is analyzed to investigate regenerative cooling characteristics and overall specific impulse. It was found that the engine can operate with the cycle. For flights at high Mach numbers, the hydrogen flow rate required for engine cooling exceeds the stoichiometric flow rate needed for combustion, and the specific impulse becomes lower than the stoichiometric combustion case.

Acknowledgments

The authors acknowledge the valuable advice from Nobuo Chinzei, the head of the Ramjet Performance Section, and Akio Kanmuri, the head of the Rocket Engine Systems Section of the National Aerospace Laboratory, Kakuda Branch.

References

[1]Buchmann, O. A., "Thermal-Structural Design Study of an Airframe-Integrated Scramjet," NASA CR-3141, Oct. 1979.

[2]Henry, J. R., and Anderson, G. Y., "Design Considerations for the Airframe-Integrated Scramjet," NASA TM X-2895, Dec. 1973.

[3]Chansler, R. C., "Hypersonic Research Engine Project—Phase

IIA/Fuel System Development/Terminal Summary Report," NASA CR-111902, Dec. 1968.

[4]Masuya, G., and Wakamatsu, Y., "Calculation of Scramjet Performance," National Aerospace Lab., Japan, NAL TR-987, July 1988 (in Japanese).

[5]Waltrup, P. J., Anderson, G. Y., and Stull, F. D., "Supersonic Combustion Ramjet (Scramjet) Engine Development in the United States," *Proceedings of the 3rd International Symposium of Air Breathing Engines*, DGLR-Fachbuch No. 6, Munich, 1976, pp. 836-862.

[6]Sutton, G. P., and Ross, D. M., *Rocket Propulsion Elements*, 4th ed., Wiley, New York, 1976, pp. 82, 282, 318, and 329.

[7]Wakamatsu, Y., Kanmuri, A., and Toki, K., "Partial Bleed Expander Cycle for Low Thrust LOX/LH_2 Rocket Engine," National Aerospace Lab., Japan, NAL TR-837T, Sept. 1984.

[8]Anderson, G. Y., Eggers, J. M., Waltrup, P. J., and Orth, R. C., "Investigations of Step Fuel Injectors for an Integrated Modular Scramjet Engine," *Proceedings of the 13th JANNAF Combustion Meeting*, Chemical Propulsion Information Agency, Applied Physics Lab., Laurel, MD, Sept. 1976.

[9]Mayer, E., "Analysis of Convective Heat Transfer in Rocket Nozzles," *ARS Journal*, Vol. 31, No. 7, 1961, pp. 911-917.

Initial Development of a Pulsed Electrothermal Thruster

Rodney L. Burton* and Shih-Ying Wang†
GT-Devices, Inc., Alexandria, Virginia 22312

I. Introduction

THE pulsed electrothermal (PET) thruster[1-4] generates stagnation pressures of tens to hundreds of atmospheres by operating in a pulsed mode. For pulse widths of 10 μs, the electrode and insulator surfaces stay below their melting points. The high operating pressure increases recombination in the nozzle to reduce frozen flow losses and exhaust gas temperatures.

The PET thruster system includes the thruster head, propellant injection system, capacitive energy storage system, power supply, and control system. The thruster head contains a cylindrical capillary discharge chamber with end electrodes, with water propellant injected along the centerline. The discharge heats the injected water to a high temperature and pressure during the pulse, creating a thrust impulse. The pulsed discharge breaks down at several hundred pulses/s to create average thrust. The 5-mm-inner-diam (ID) × 56-mm-long cylindrical capillary insulator is made of prestressed silicon nitride or alumina[4]; smaller boron nitride insulators with 4- and 3.2-mm ID were also used.

The PET thruster head is water cooled, enabling thermal heat loss to be measured calorimetrically. The thruster is not sensitive to electrode polarity and is operated here with the propellant injected through the anode at the stagnation end. The grounded cathode is located at the sonic throat. The anode material is 0.15% alumina dispersion-strengthened copper or sintered tungsten alloy. The 400:1 contoured exhaust nozzle contains the tungsten alloy cathode as an insert.

Water propellant is continuously injected through a straight 75-100 μm orifice with an L/D (length/diameter) of 1.5-5.0. At 200-400 pulses/s, the propellant only travels a few centimeters between pulses, so that injected, unevaporated liquid is heated by two or three pulses. The water is injected either as a straight jet or atomized spray. A finite element thermal model is used to predict and avoid the onset of boiling at the orifice. A ceramic Macor thermal insulator prevents propellant boiling when operating near the ideal propellant flow. The water flow requirement for the PET thruster at 1500-s specific impulse is 6 mg/s/kW, giving 60 μg/pulse at a typical pulse rate of 100 pulses/s/kW.

Spray injection is achieved through the technique of aerated liquid atomization.[5] Helium gas is introduced upstream of the orifice, with the liquid and gas passing through the orifice as a mixture, producing a fine 20 μm spray with a total spray angle of 15-20 deg. This approach uses a gas mass flow rate of 1-10% of the liquid mass flow rate. The resulting aerated liquid spray intersects the hot wall of the capillary where the droplets are partially evaporated, forming a vapor film that prevents further wall contact.

Based on studies of droplets exposed to gas dynamic shock waves,[6] it is probable that axial vapor flow causes the drops to shatter on a time scale of a few μs. The Weber number $\rho u^2 d/\sigma$ for 20 μm drops is $We = 2 \times 10^3$ near the throat, greatly exceeding the critical Weber number $We \approx 5$. This shattering process is crucial to the coupling between the water and the discharge.[7]

The thruster is driven at 200-400 pulses/s by a 10 section, 10 μF, 0.48 Ω pulse-forming network (PFN), using phenyl xylyl ethane (PXE) dielectric capacitors with an estimated dielectric loss of 0.2 W at 5 kW. Predicted life is 10^9-10^{11} pulses. Demonstrated life here is $> 2 \times 10^7$ pulses with zero failures and 10^{11} pulses in a similar application, so that capacitor life is no longer considered an issue for the PET thruster. The PFN is designed to match the electrical resistance of the discharge and to prevent electrode or insulator surface melting during the pulse.[4] The thruster is tested with axis vertical on a 1 m^3 vacuum tank, with a tank pressure of 1 Torr.

II. Operational Tests

Tests were run at the several-kilowatt level to measure thruster operating parameters. Test experience with 56-mm-long ceramic insulators is summarized in Table 1, covering 26.6×10^6 total pulses.[4]

Insulator ablation was measured with dimensional gauge pins after each test. In no case was any erosion observed with Si_3N_4, Al_2O_3, or BN. Although the insulators experienced sputtering from the eroding electrodes, no dimensional change was detected and no change in electrical behavior was observed.

Electrode erosion was measured for thruster average power of 1.3-3.6 kW. Electrode mass loss for the PET thruster is plotted vs average thruster power in Fig. 1, covering a variety of anode geometries, anode materials, and arc conditions. Because plasma heat transfer does not cause electrode surface melting, the observed erosion is probably due to coulombic charge transfer. Experimental measurements for vacuum arcs show[8,9] that charge transfer erosion decreases with pressure to 2-3 μg/C at 500 Torr. Most of the present data fall below 10 μg/C, much of it in the 2-4 μg/C range, with cathode erosion

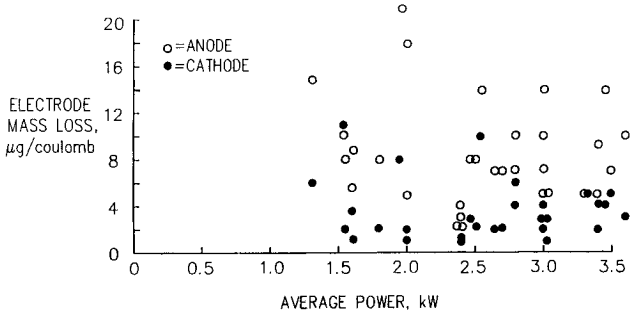

Fig. 1 Electrode mass loss, showing lower erosion for the cathode.

Presented as Paper 89-2265 at the AIAA 25th Joint Propulsion Conference, Monterey, CA, July 10-12, 1989; received Dec. 1, 1989; revision received May 5, 1990; accepted for publication June 7, 1990.

*Director, Space Applications; currently Associate Professor, Department of Aeronautical and Astronautical Engineering, University of Illinois, Urbana, IL. Member AIAA.

†Senior Scientist.